CAAP Quarterly Report

Date of Report: July 10, 2015

Contract Number: DTPH56-14-S-N000006

Prepared for: Government Agency: DOT

Project Title: Laser peening for preventing pipe corrosion and failure

Prepared by: Board of Regents of the University of Nebraska for the University of Nebraska–Lincoln

Contact Information: Yongfeng Lu
Lott Distinguished Professor
Department of Electrical and Computer Engineering,
University of Nebraska-Lincoln,
209N Walter Scott Engineering Center,
Lincoln, NE 68588-0511
Phone: (402) 472-8323
E-mail: ylu2@unl.edu

For quarterly period ending: June 30, 2015

Business and Activity Section

(a) Status Update of Past Quarter Activities

1. The major goal of the project

The ultimate goal of this project is to investigate and develop laser peening of pipeline steels to improve the corrosion resistance of stainless steel and carbon steel used for pipeline construction. The corrosion resistance of pipelines will be enhanced *via* the compressive residual stress created by laser-induced shock waves during laser peening. It is anticipated that by using laser shock peening in the construction of a pipeline, the reliability, safety, and lifespan of the nation's pipeline transportation system will be highly improved. As stated in our proposal, the major

goals of this project include four phases and associated objectives. Table 1 summaries the progress achieved during this reporting period for each objective in each phase.

Table 1. The completion rate for each objective in each phase of the project.

Phases	Major goals and milestones	Starting date (mm/dd/yy)	Ending date (mm/dd/yy)	Completion rate (%)
Phase 1	1) Experimental setup for laser cleaning developed	10/01/2014	12/31/2014	100
	2) Cleaning mechanism and parameter windows	01/01/2015	09/30/2016	0
	3) Real-time monitoring of cleaning process	01/01/2015	09/30/2016	0
Phase 2	1) A laser peening system developed	10/01/2014	12/31/2014	100
	2) Parameter windows for laser peening established	01/01/2015	09/30/2016	60
Phase 3	1) Surface morphology study of the laser-peened surfaces	01/01/2015	09/30/2016	60
	2) The residual stress of pipeline steels after laser cleaning and peening	01/01/2015	09/30/2016	40
	3) The corrosion resistance of laser-peened surface	01/01/2015	09/30/2016	10
Phase 4	Design a laser peening prototype system	06/30/2016	09/30/2016	0

2. The specific objectives during this reporting period

During this reporting period (April 1, 2015, to June 30, 2015), the microhardness distribution of laser-peened samples along the near-surface region and the depth direction have been investigated. In addition, the microstructural features of the laser-peened samples have been characterized by optical microscopy (OM), scanning electron microscopy (SEM), and transmission electron microscopy (TEM). Finally, an initial study on the effects of laser shock peening (LSP) on stress corrosion cracking (SCC) has been carried out. The phased objectives and specific content are as follows:

(1) The effects of multiple LSP impacts on microhardness distribution for stainless steel (SS) and carbon steel (CS).

(2) Sample preparation for microstructure observations.

(3) The effect of LSP on the changes in microstructures of treated samples in the shocked region.

(4) Sample preparation for proof ring testing.

(5) SCC constant load testing and analysis.

3. Response to the comments

Comment 1: Pg.4: 1.99% C, 0.30% W is not carbon steel. Also, S is too high! Perhaps OES chemistry, which is more precise, should also be performed. Others indicate that OES is a better quantitative method to characterize metal samples, although if they are looking to retain surface properties OES will disrupt (burn/heat) the surface and change grain morphology. Other suggestions are that EDX (or EDS – Energy Dispersive Spectroscopy) is a touchy technology and yet is more qualitative than quantitative except under optimal conditions (perfectly flat/clean sample with good calibration samples, a very experienced operator, and careful interpretation of spectra since curve fitting is an art that the computer is happy to try it's best at). Most SEMs are set up to use a tungsten filament, so I was thinking initially maybe it was a backscatter phenomenon giving them the tungsten, but looking at the spectrum they included, I think they are letting the software do curve fitting, and coming up with the wrong elements such as fluorine and tungsten (lack of Beta peaks where they have W marked on the spectrum that's included). Further, it states they used 5kV for the SEM… I recall higher Voltages helped with EDS (we used 20-30kV, but on a substandard SEM).

Answer: Thank you very much for your detailed comments. We totally agree with you. Energy dispersive spectroscopy (EDS) is indeed a touchy technique and is more qualitative than quantitative. It is also not very sensitive to trace elements with a weight ratio of less than 0.5%, especially for lighter elements such as carbon, sulfur, and nitrogen. Though optical emission spectroscopy (OES) is a better quantitative method for characterizing metal samples, this equipment is not available at our institution. If necessary, we will discuss purchasing one for our lab. We think that the erroneous EDS measurement result obtained last time was mainly due to the following reasons: (1) nonoptimized test conditions, such as voltage; (2) low energy carbon X-ray K line which meant that only the carbon x-ray from the surface of the specimen could be counted; and (3) there could be a significant carbon background signal from the chamber surfaces. To reduce the measurement error and to estimate the relative content of carbon and sulfur in the carbon steel, a further EDS measurement was carried out under optimal test conditions (voltage: 20 kV). As a reference, one piece of standard stainless steel material with certified element composition was also measured under the same conditions. Table 2 shows the chemical compositions of carbon steel and standard stainless steel. For the standard stainless steel, most of the relative content of the elements were very close to the standard value, except for some of the lighter and trace elements, such as carbon and nitrogen. For the carbon steel sample, only carbon (1.16%), manganese (0.27%), sulfur (0.02%), and iron (98.54%) were detected. Compared with the measurement results for stainless steel, the actual carbon content in carbon steel must be much lower than 1.16%; and it was estimated to be at the level of 0.02%. In addition, no fluorine and tungsten elements were detected this time; and the relative sulfur content was approximately 0.02%. In general, EDS can be used to preliminarily estimate the

chemical composition of carbon steel under optimal test conditions and by finding a standard sample as a reference.

Table 2. Chemical compositions of the standard stainless steel (wt.%)							
Composition	Fe	Cr	Ni	Mn	Cu	Mo	Si
Standard (wt. %)	69.95	18.17	8.19	1.83	0.66	0.47	0.28
Measured (wt. %)	68.36	18.05	7.89	2.05	0.66	0.43	0.20
Composition	Co	V	N	W	P	S	C
Standard (wt. %)	0.14	0.07	0.06	0.05	0.04	0.03	0.02
Measured (wt. %)	0.23	0.09	0.00	0.25	0.00	0.05	1.50
Composition	Cb	Sn	Ta	Al	Ti		
Standard (wt. %)	0.02	0.01	0.01	0.01	0.003		
Measured (wt. %)	0.00	0.02	0.20	0.02	0.000		
Chemical compositions of the carbon steel (wt.%)							
Composition	C	Al	Si	Mn	W	S	Fe
This time (wt. %)	1.16	0	0	0.27	0	0.02	98.54

Comment 2: Pg.5: Was actual tensile testing performed? If so, please provide details of test.

Answer: No, we didn't perform the actual tensile testing in our lab. The mechanical performance parameters (tensile strength, yield strength, and elongation, etc.) were provided by a product supplier.

4. Significant results

4.1 Experimental

4.1.1 Principle and experimental LSP procedure

LSP is a cold mechanical process where pressure waves caused by expanding plasma plastically deform the surface of a material. LSP uses a thin layer of ablative material that is opaque to the laser. The opaque ablative material, typically black spray paint or tape, was used as a sacrificial layer in an early study by Fairland and Clauer [1]. The sacrificial layer also minimizes thermal effects on the surface caused by the laser. The laser partially vaporizes the ablative layer to form high pressure plasma. The plasma, confined by a thin layer of water film (confining medium), expands rapidly resulting in a recoiling pressure wave on the order of GPa reported by Fariland et al. and Caslaru, et al. [2-3] The pressure wave is a cold mechanical process that typically deforms the surface. The plasma-induced shock pressure causes severe plastic deformation, refined grain size, compressive residual stresses, and increased hardness at the surface and in the subsurface. As a result, the mechanical properties on the workpiece surface are enhanced to improve the prevention of corrosion and foreign object damage.

4.1.2 Experimental material and parameters

During this reporting period, the samples tested were prepared from 304SS and CS. The 304SS and CS test samples were both cut into a 10×10×2 mm^3 (width × length × thickness) rectangular shape. Prior to the LSP treatment, the samples were mechanically polished with sand paper of different grades (400 to 1200) and polishing powders (3 μm, 0.3 μm) to achieve a mirror-like surface, to enable the microhardness test, metallographic imaging, and TEM, which requires a low surface roughness of several hundred nanometers. The polishing was followed by ultrasonic cleaning with acetone/methanol to degrease the sample surface. All samples were prepared shortly before the LSP experiments.

The main LSP process parameters are listed in Table 3. The laser source is a continuum Q-switched Nd:YAG PR II 8010 laser. During this quarter, laser pulses with a wavelength and energy of 1064 nm and 850 mJ were used. Black tape with a thickness of 177 μm was used as the sacrificial layer. In order to avoid the influence of the water spray induced by laser ablation during laser-material interaction, a focusing lens with a focal length of 50 cm was used. Two different LSP experiments were designed: a single-spot LSP experiment and a large-area LSP experiment, from which two kinds of laser-peened samples were obtained.

Table 3. The processing parameters used in the LSP experiment.

Type	Values
Laser type	Continuum Nd:YAG PR II 8010 laser
Laser pulse energy (mJ)	850
Pulse duration (nm)	6 ~ 8
Frequency (Hz)	1 ~ 10
Wavelength (nm)	1064
Laser beam size (mm)	~ 1
Sacrificial coating	Black tape (177 μm)
Confining medium	Flowing water (1 ~ 2 mm)

4.1.3 Sample preparation for microhardness measurement and microstructure observation

After the LSP experiments, cross-sections perpendicular to the sample surface were cut for microhardness measurement along the depth direction and for metallographic investigation. The detailed process is described as follows: (1) the sample surfaces were processed by single-spot or large-area laser peening; (2) the samples were then attached to the holders with superglue, cut (using ISOMet 1000 Precision Saw), and ground along their cross-sections to the needed position; and (3) the cross-sections of the samples were polished mechanically with sandpaper of different grades (400 to 1200) and polishing powders (3 μm, 0.3 μm) to achieve a mirror-like surface.

The micromechanical properties of all samples tested were determined using a Tukon 2500 Vickers & Knoop microhardness tester with a square-based diamond pyramid indenter. To perform metallographic observation, the cross-sections of the samples were etched to show grain boundaries and different phases using a specific reagent. For 304SS, aqua regia (volume ratio of

HCl to HNO_3: 3:1) was adopted; for CS, nital, consisting of 4% HNO_3 and 96% ethanol, was used. The etched cross-sections of the samples were then characterized by an optical microscope (Nikon ECLIPSE, Japan) and a scanning electron microscope (Philips, XL 30E, 5kV).

In addition, the microstructural changes in a laser-peened sample surface were characterized using a transmission electron microscope (JEOL 2010, Japan). The TEM samples were prepared using the following steps: (1) the front surface of the sample ($10\times10\times2$ mm^3) was processed by large-area laser peening for predetermined times; (2) the processed samples were cut parallel to the laser-peened surface to decrease the sample thickness from 2 to approximately 1 mm; (3) the samples (front surface) were attached to the holder with superglue, ground from the back face to decrease the sample thickness to about 150 μm, and polished to a mirror-like surface with sandpaper and polishing powder; (4) the samples were detached from the holder by ultrasonics with acetone, and the back surface was attached to the holder to polish the front surface with polishing powder only; (5) the samples were detached from the holder and cleaned by ultrasonics with acetone; (6) the thin slides were punched to get small wafers of the diameter of 3 mm; and (7) a double-jet electropolishing machine was used to generate an ultrathin area with a thickness of approximately 100 nm near the center of the small wafers.

The double-jet electropolishing procedures are described as follows: (1) three glass dishes with filter paper wetted by solutions (two with methanol and one with ethanol) were prepared and a beaker of methanol was filled with liquid nitrogen to cool it down; (2) an electropolishing solution (5% perchloric acid (70%) and 95% methanol for 304SS) was prepared; (3) the solution was poured into the electropolishing tank and liquid nitrogen was added to cool down the solution to approximately -20 ^{o}C; (4) the wafer sample was fixed on the holder which was installed on the electropolishing machine; (5) the current-voltage curve was obtained by auto-test, and suitable voltage in the flat region was determined; (6) the double-jet electropolishing machine did the formal polishing automatically; (7) as soon as the polishing was finished, the sample was dipped into the low-temperature methanol in the beaker for 1 min and then the dishes for residual solution were removed; and (8) the sample was removed from the holder. Note that a successful sample should be shining with a small hole/holes near the center.

4.2 Results and discussion

4.2.1 The effect of LSP on microhardness distribution for 304SS and CS

The improvement of material hardness is one of the most important characteristics of laser shock peening. The changes in hardness could generally reflect the effectiveness of the LSP process in one respect, which is considered to be induced by microstructural change. Therefore, in the last quarterly report, microhardness changes of stainless steel, carbon steel, and Al alloy after laser peening were initially investigated at the center of the LSP-induced dent on the sample surfaces. An obvious increase in microhardness and its dependence on laser shock peening impact times

were observed, the first step in revealing the LSP effect on microhardness change. To deepen this research during this reporting period, microhardness distributions of stainless steel and carbon steel samples along the surface direction and the depth treated by single-spot and large-area LSP were systemically investigated using a Tukon 2500 Vickers hardness tester. The stainless steel and carbon steel samples were prepared according to the procedure described in Section 4.1.3.

The load curves on the cross-section were obtained before the real test for both 304SS and CS. As shown in Fig. 1, 0.3 kg at the flat region of the load curve was selected as the load value for both of the materials. The results of microhardness distribution for single-spot LSP and large-area LSP will be discussed separately in this section.

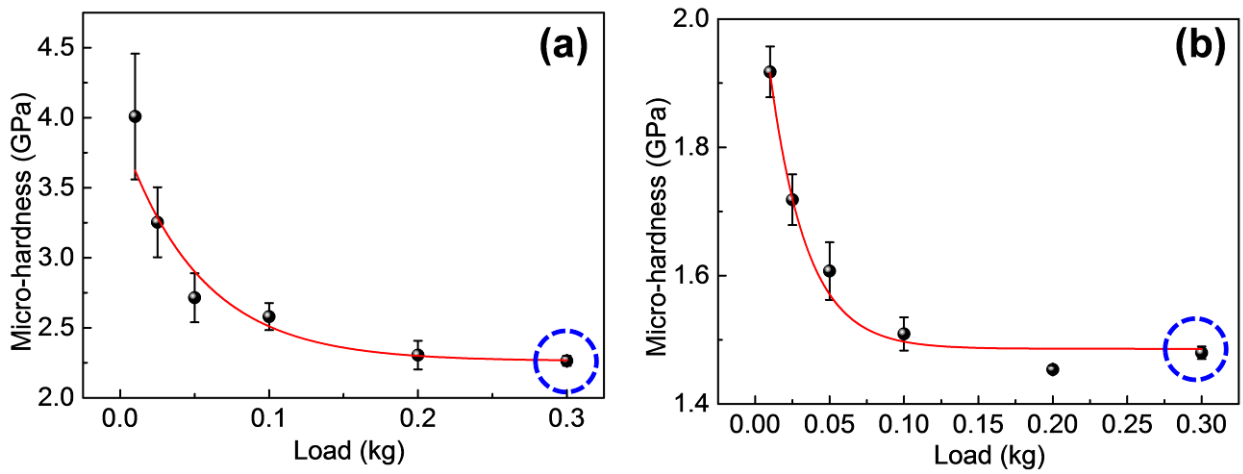

Fig. 1. Load curves for (a) 304 SS and (b) CS.

A. Variation of microhardness after single-spot LSP

The 304SS sample was first processed by single-spot laser shock peening for one to five impact times. Figure 2(a-d) shows the surface morphologies of the single-spot LSP-induced dents with (a) one, (b) two, (c) three, and (d) five impacts, respectively. After LSP, cutting, grinding, and polishing, as described under sample preparation, were performed to obtain the cross-sections across the center of the LSP-induced dents. The surface morphologies of the samples after cutting, grinding, and polishing are shown in Figs. 2 (e-h), corresponding to the images in (a-d). The dependence of dent depth on pulsed laser impacts for 304SS before and after cutting is shown in Figs. 2(i) and 2(j), respectively. With one, two, and three impacts, the dent depths nearly retained the same value, indicating a good cross-section location near the dent centers. With five LSP impacts, the dent depth decreased slightly, showing a small deviation of the cross-section location from the dent center.

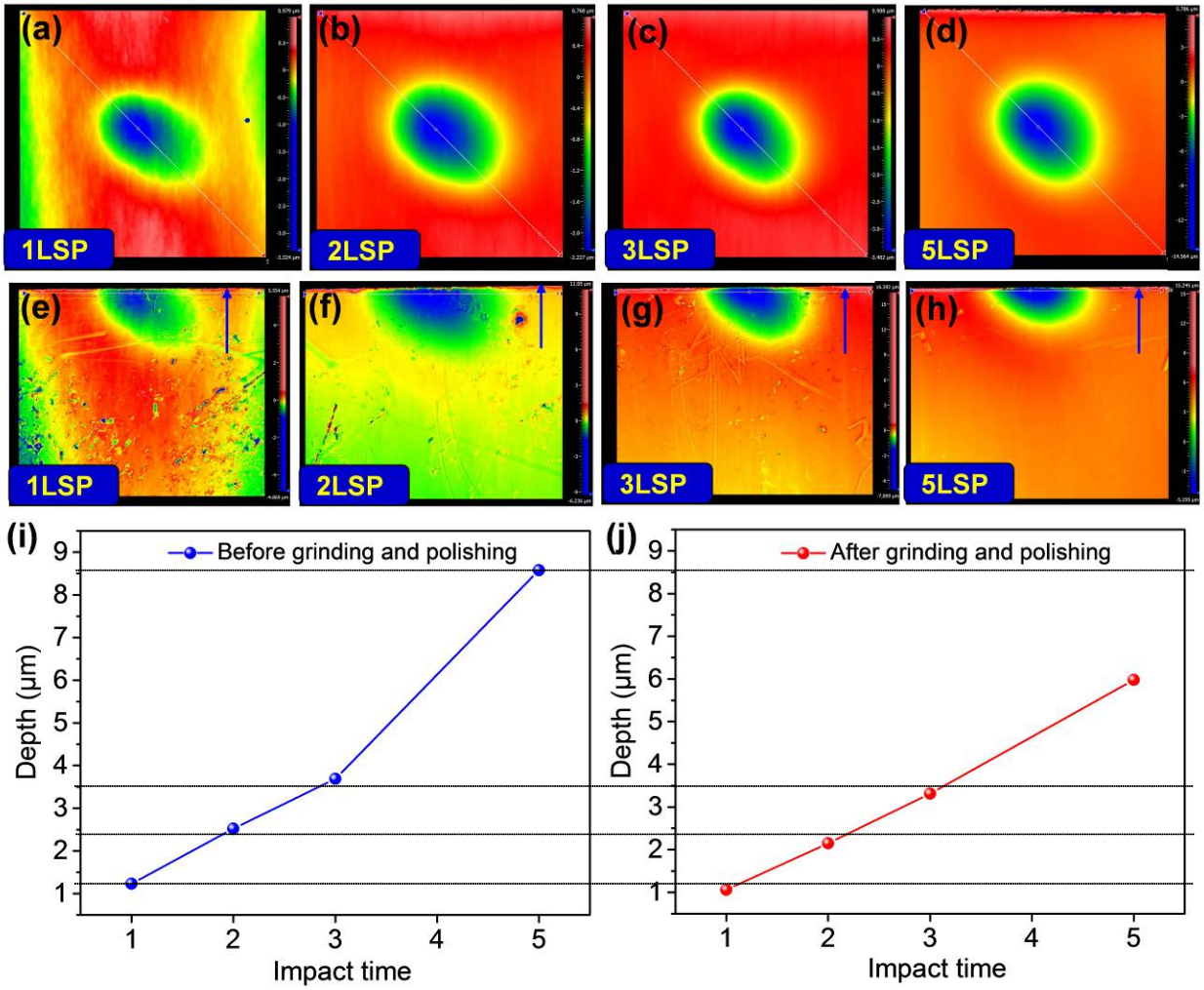

Fig. 2. (a-d) 3D surface topographies of the 304SS surfaces treated by single pulse LSP for (a) one, (b) two, (c) three, and (d) five impacts. (e-h) The corresponding 3D surface topographies of 304SS in (a-d) after cutting, grinding, and polishing along the near-center line of the laser-peened regions. The arrows in (e-h) point to the edges of the samples. Dependence of dent depth on pulsed laser impacts for 304SS (i) before and (j) after cutting, grinding, and polishing.

After finding the cross-section position located along the center line of the LSP-induced dents, the cross-sectional microhardness distribution was measured by a Vickers microhardness tester. As shown in Fig. 3(a), both the hardness distribution along the surface direction and the depth were obtained to generate the two-dimensional (2D) microhardness distribution on the selected cross-section region. The microhardness distribution results for two, three, and five LSP impacts are shown in Fig. 3(b), (c), and (d), respectively. It can be seen that the highest hardness was obtained near the laser-peened surface (100 μm depth) and with five LSP impacts. There was no obvious microhardness improvement for two and three LSP impacts. Figure 3(e) shows the 3D cross-sectional microhardness distribution mapping treated by five impacts, indicating a clear hardness distribution along the surface and depth direction, where the top surface and center of

LSP-induced dents have the maximum values of microhardness. In general, the microhardness increased with the increment in LSP impacts and decreased rapidly with increased depth.

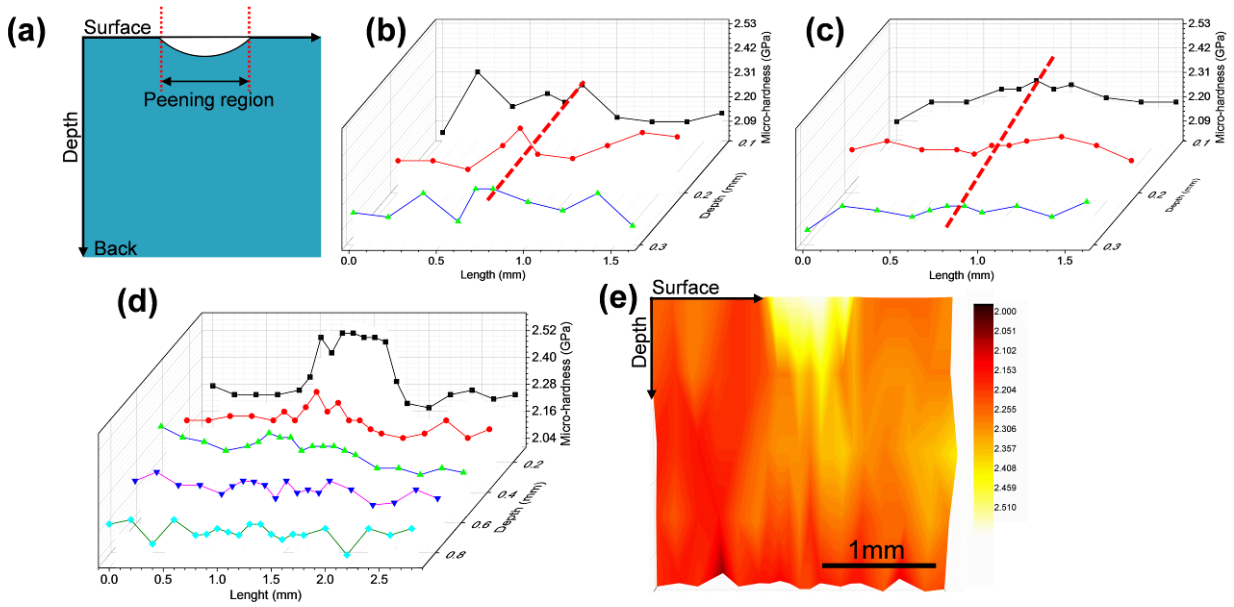

Fig. 3. (a) Schematic of the cross-section of a 304SS sample treated by LSP. The microhardness distribution along the surface and depth treated by single-spot LSP for (b) two, (c) three, and (d) five impacts. (e) 3D cross-sectional microhardness distribution treated by five impacts.

In Fig. 4(a), the profiles of the dent depth and the corresponding cross-sectional hardness distribution along the subsurface (100 μm depth) with five single-spot LSP impacts were put together for comparison, with the dashed black line indicating the dent center. The dent depth was nearly a Gaussian profile with a center depth of about 6 μm and a diameter of about 1.2 mm. On the other hand, the microhardness distribution showed a flat top close to the dent center with a length of about 0.6 mm; and the microhardness increased sharply from substrate value to the highest value within 0.2 mm on each side. Figure 4(b) shows the microhardness distribution for the 304SS sample along the depth direction after multiple LSP impacts. It can be observed from Fig. 4(b) that the significant and maximum microhardness mainly exists in the subsurface region for different numbers of LSP impacts. Increasing LSP impacts has remarkably improved the microhardness at different depths from 100 to 900 μm, while the values with one and two LSP impacts have some deviation. Since the microhardness value at 900 μm is still higher with LSP compared to an as-received sample, the depth affected by single-spot LSP must be deeper than 900 μm, which needs to be confirmed by hardness profiles at deeper positions and repeated experiments in future research work.

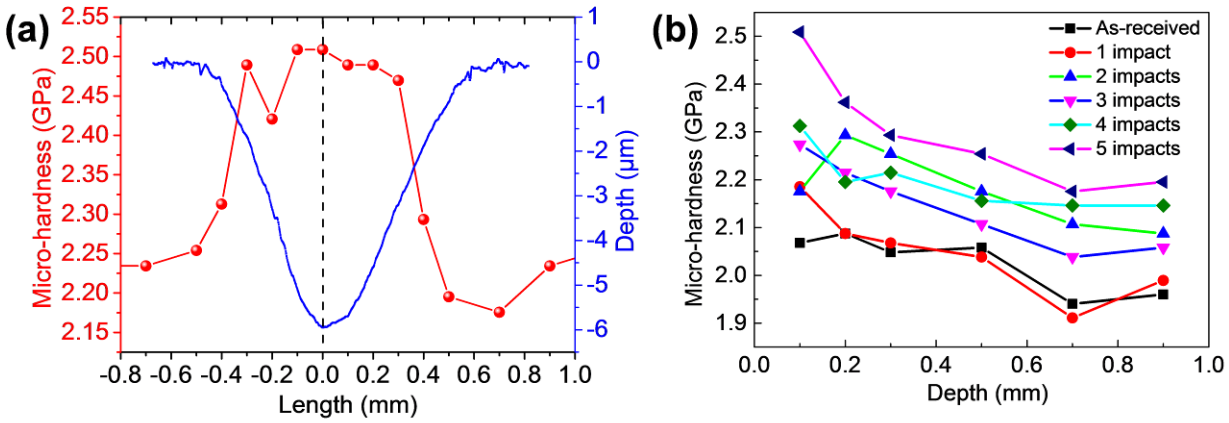

Fig. 4. (a) The microhardness distribution along the near surface and dent depth treated by five impacts. (b) Microhardness profiles of 304SS along the depth direction after multiple LSP impacts with the number of impacts.

B. Variation of microhardness after large-area LSP

The cross-sectional microhardness distribution of the samples after large-area LSP has been investigated.

Figure 5 shows the microhardness distribution along the subsurface direction (at 100 μm depth) for (a) 304SS and (b) CS. In Fig. 5(a), the microhardness of 304SS shows an obvious improvement from the no-LSP area to the LSP area. In addition, with the incremental LSP impacts, the microhardness increased rapidly. For one, four, and eight LSP impacts, the average microhardness was 2.24, 2.47, and 2.70 GPa, respectively, which was approximately 1.1, 1.2, and 1.3 times higher than that of the no-LSP area (2.04 GPa). In the LSP area, although the laser spot size was 1 mm, the microhardness did not show obvious periodic fluctuation, which means a relatively uniform processing effect could be achieved at the selected overlapping rate of 50%. The uniform microhardness distribution might also have been related to the flat top hardness phenomena that we observed in the single-spot LSP experiment. For carbon steel results in Fig. 5(b), the increase in hardness was not obvious under the same LSP conditions used for 304SS. The original average microhardness of the carbon steel was only approximately 1.57 GPa, which was much lower than that of the as-received 304SS (2.04 GPa). After one, four, and eight LSP impacts, the average microhardness increased to 1.58, 1.59, and 1.67 GPa, respectively. It should be noted that, compared to the 304SS with higher hardness, the carbon steel with lower hardness was much less hardened by laser shock peening under the same processing parameters. The microstructure, such as the grain size and phase difference, might be the reason, which will be explained by the following metallographic investigation (see Section 4.2.2).

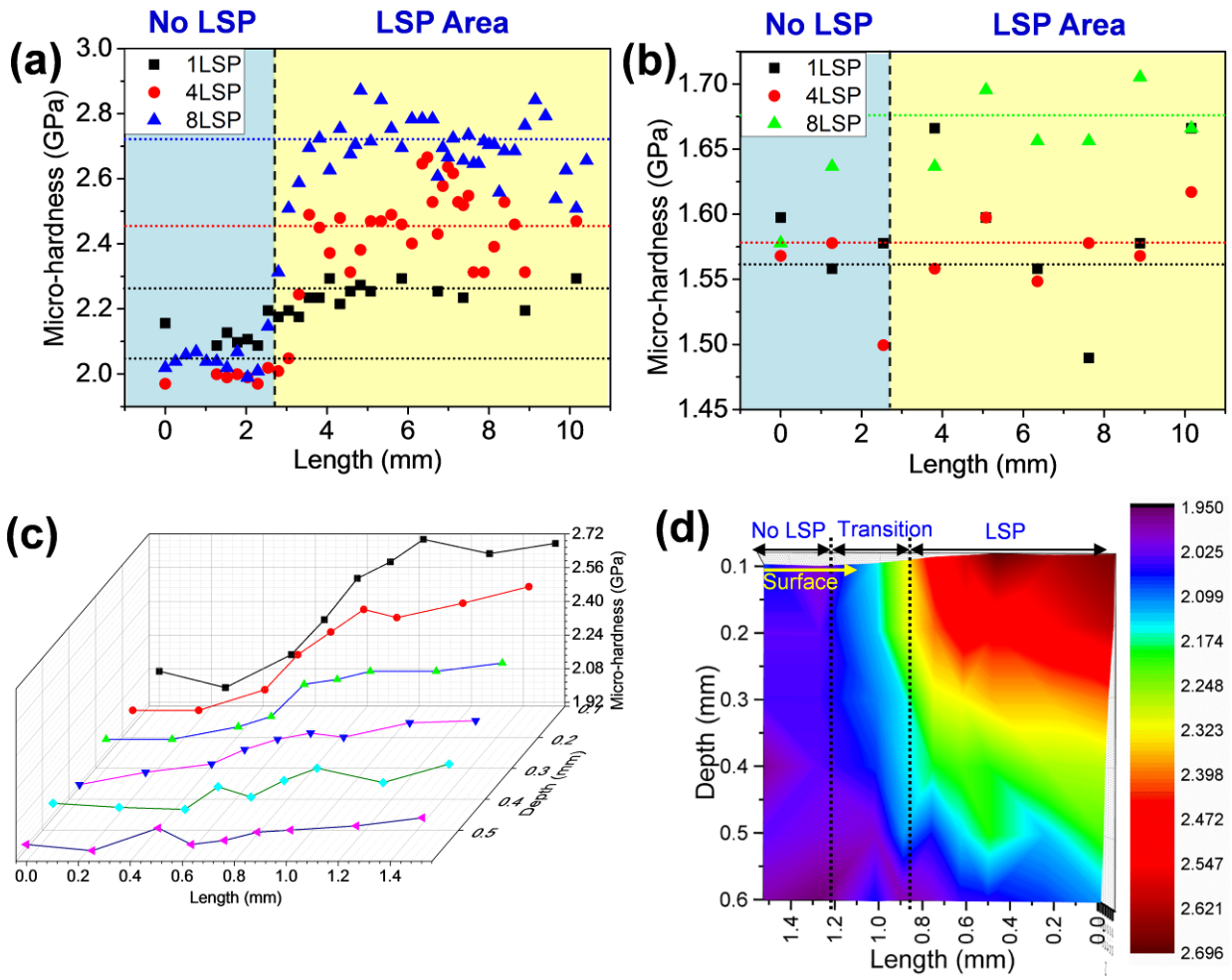

Fig. 5. Microhardness distribution of (a) 304SS and (b) CS along the near surface from no-LSP area to LSP with the number of impacts. (c) 2D and (d) 3D cross-sectional microhardness distribution along the depth across the transition area (from no-LSP area to eight LSPs area).

Due to the significant hardness increase of 304SS by four and eight LSP impacts, the transition from the no-LSP area to the LSP area could be identified. The length of the transition area with four large-area LSP impacts was approximately 200 μm, which was similar to that with five single-spot LSP impacts. For eight LSP impacts, the transition area was approximately 400 μm, which was much longer than that with four LSP impacts. A detailed cross-section microhardness distribution along the depth across the transition area from the no-LSP area to the eight LSP impacts area is shown in Fig. 5(c) and (d). For different depths (less than 0.5 mm), the length of the transition area remained the similar value of approximately 400 μm, while the hardness gap between the LSP and no-LSP area decreased with increased depths. At a depth of 600 μm, no obvious hardness difference could be observed between the no-LSP area and eight LSP impacts area. The above results could be attributed to the expansion of the affected region due to multiple LSP impacts.

Figure 6 shows the microhardness distribution along the depth for (a) 304SS and (b) carbon steel treated by multiple large-area LSP. It can be seen from Fig. 6(a) that, similar to the single-spot LSP, the near-surface microhardness of 304SS increased the most obviously with the increment of LSP impacts; and the microhardness decreased rapidly with the increased depth. When the depth was less than 500 μm, the microhardness was higher with more LSP impacts. With a depth between 500 μm and 700 μm, the LSP-induced hardness improvement vanished. For deeper positions, the magnitude of microhardness did not change and was almost not influenced by the impact time. For carbon steel, as shown in Fig. 6(b), the near-surface microhardness increased a little with the incremental LSP impacts, much lower than 304SS. The low microhardness increase of carbon steel confirmed the microhardness results along the surface direction, which might have been induced by the microstructure difference between 304SS and carbon steel.

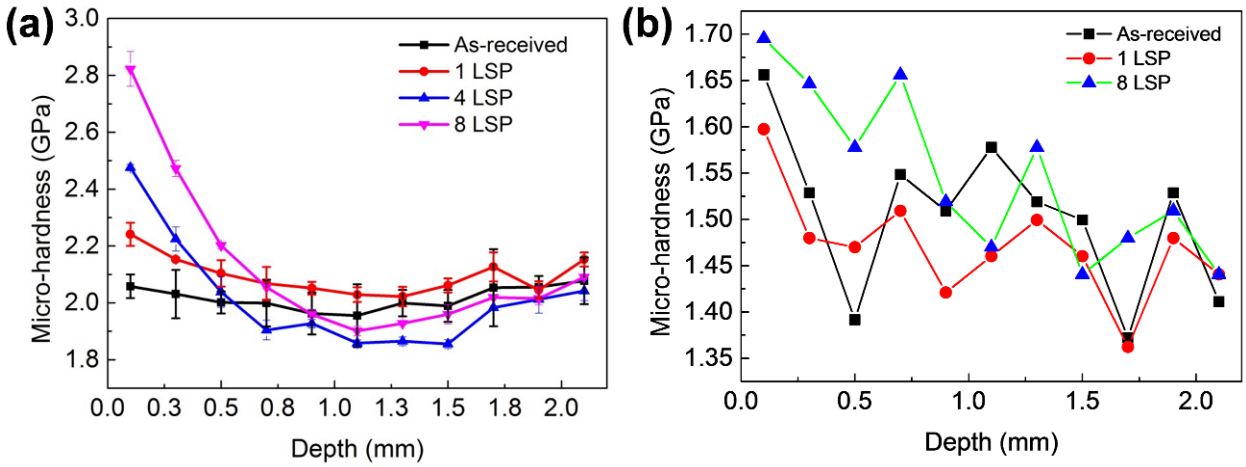

Fig. 6. Microhardness profiles of (a) 304SS and (b) CS after multiple large-area LSP impacts with different numbers of impacts.

4.2.2 The effect of LSP on microstructures in the shocked region

Metallography is essential in the study of the structural characteristics or constitution of a metal or an alloy in relation to its physical and mechanical properties. Metallographic examination can provide quantitative information about the specimen's grain size, amount of interfacial per unit volume, and the amount and distribution of phases. In this reporting period, metallographic observation was used for microstructure investigation in combination with the microhardness results. For metallographic observation, the polished sample should be etched by special solutions to allow the microstructures show up. As stated in Section 4.1.3, aqua regia and nital were used for 304SS and carbon steel etching, respectively. After etching, both the OM and SEM were used for imaging.

A. OM and SEM observation

Figure 7(a) and (b) shows the optical images of the etched surfaces of 304SS and carbon steel without laser peening, respectively. The 304SS sample shows austenite structures (Fig.7a). Carbon steel shows white ferrite structures with some black areas around the grain boundaries (Fig.7b), which is suspected to be the secondary phase. To further confirm and identify the microstructures, SEM observation was needed. Figure 7(c) shows the SEM image of the surface of the etched 304SS sample, where only an austenite structure phase is observed; and the average size on the surface is about 11 μm, which is similar to optical imaging results. From the SEM observation (Fig. 7d), the black areas of the carbon steel in the optical imaging (Fig. 7b) correspond to lamellar structures in SEM imaging, which are most likely to be the pearlite. Therefore, carbon steel probably consists of two phases, ferrite and pearlite, respectively. In addition, the existence of a pearlite phase is considered to be one of the important reasons for the difficult-to-change hardness of the carbon steel with laser shock peening.

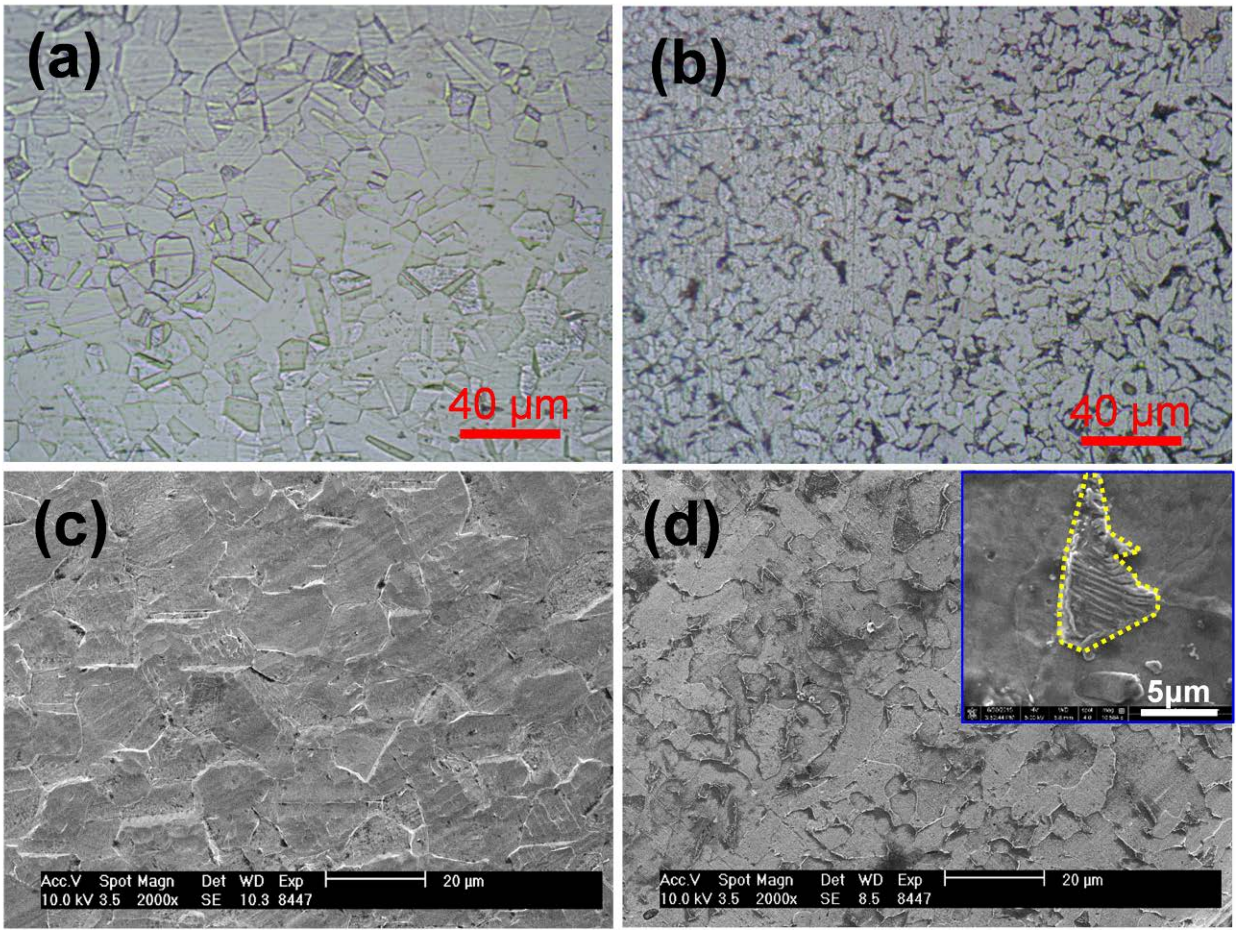

Fig. 7. Optical images of microstructures of original (a) 304SS and (b) CS after etching. (c) and (d) the corresponding SEM images of the samples shown in (a) and (b), respectively. Inset in (d) shows an enlarged SEM image.

Cross-section samples after multiple large-area LSP impacts were used for metallographic investigation. Figure 8 shows typical optical images of the cross-sections of the 304SS (a) before and (b-d) after laser peening for (b) one, (c) four, and (d) eight impacts. The areas used for observation were near the laser-peened surfaces, where the laser peening should be the most effective for microstructural changes. Figure 9 shows cross-sectional SEM images with different magnification of 304SS (a-c) before and (d-f) after laser peening for eight impacts. Grain boundaries are marked by dashed yellow lines in SEM images under the highest magnification (Fig. 9c and f). Comparing the SEM images of the samples before and after laser peening, no obvious changes are observed in the grain size. However, some laminar structures can be clearly observed in the sample treated by eight LSP impacts, which may be twins generated by shock wave impacts. Through the extended optical and SEM images, the quantitative grain sizes are determined by making lines and counting the intersection numbers. For each grain size achieved, eight lines at four different images were counted. The average grain size of the sample before laser peening was about 10.5 μm, while those after LSP for one, four, and eight impacts were 9.84, 8.9, and 8.82 μm, respectively. Although the grain size did not show great change, other factors, such as the increase of twin and dislocation density, also contributed to the microhardness increase we measured. On the other hand, the small change in the grain size might be attributed to the low laser power density. Lasers with higher pulse energy and better focusing systems should be used in the future to enhance the LSP effects.

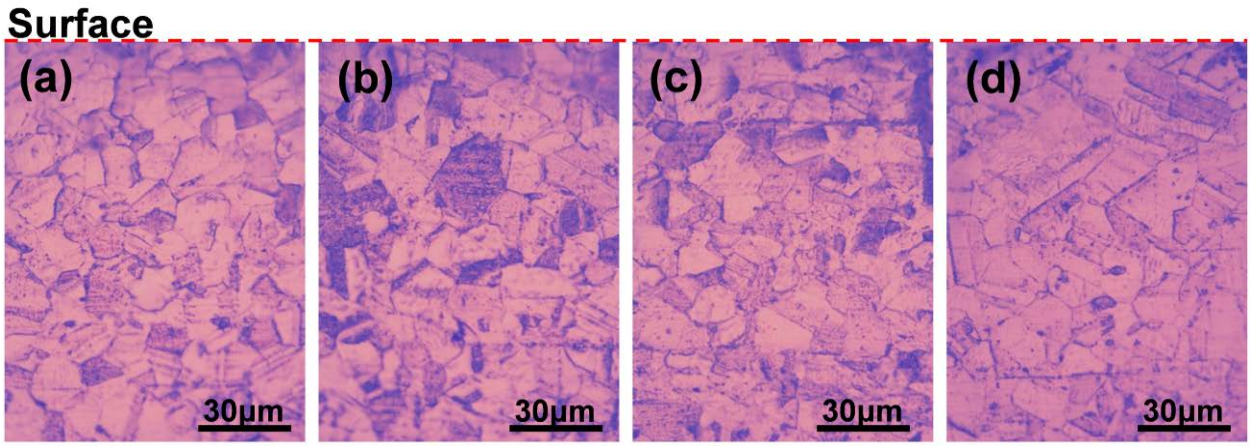

Fig. 8. Optical images of the cross-sectional microstructures of 304SS (a) before and (b-d) after laser peening for (b) one, (c) four, (d) eight impacts.

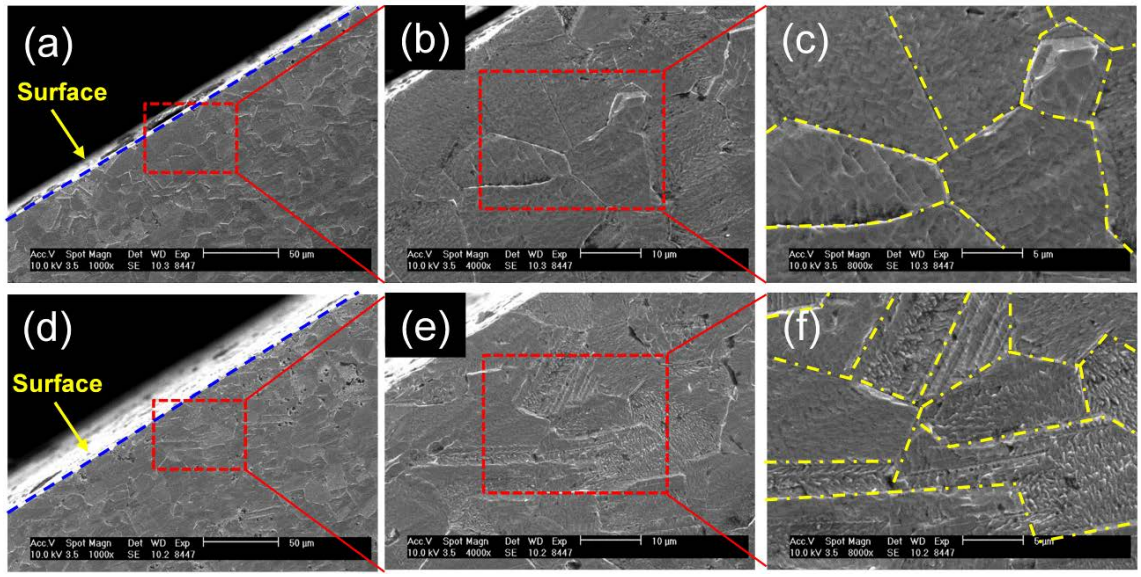

Fig. 9. Different magnified SEM images of the cross-sectional microstructures of 304SS (a-c) before and (d-f) after laser peening for eight impacts.

Figure 10(a) shows the optical images of carbon steel (a) before laser peening, and Fig. 10(b-d) shows the optical images with (b) one, (c) four, and (d) eight LSP impacts. Figure 11 shows the SEM images with different magnification for 304SS (a-c) before and (d-f) after laser peening for eight impacts. The dashed yellow lines in the SEM images with the highest magnification indicate the grain boundaries. In the same way we examined 304SS, the average grain size (only for the ferrite) of carbon steel was determined to be 6.63 μm before laser peening and decreased to 6.36 μm after eight LSP impacts. The nearly unchanged grain size of the CS agrees well with the tiny change in the micro-hardness before and after LSP processing. Moreover, the grain size of CS is much smaller than that of 304SS which may be another reason for the barely changed hardness even with eight LSP impacts.

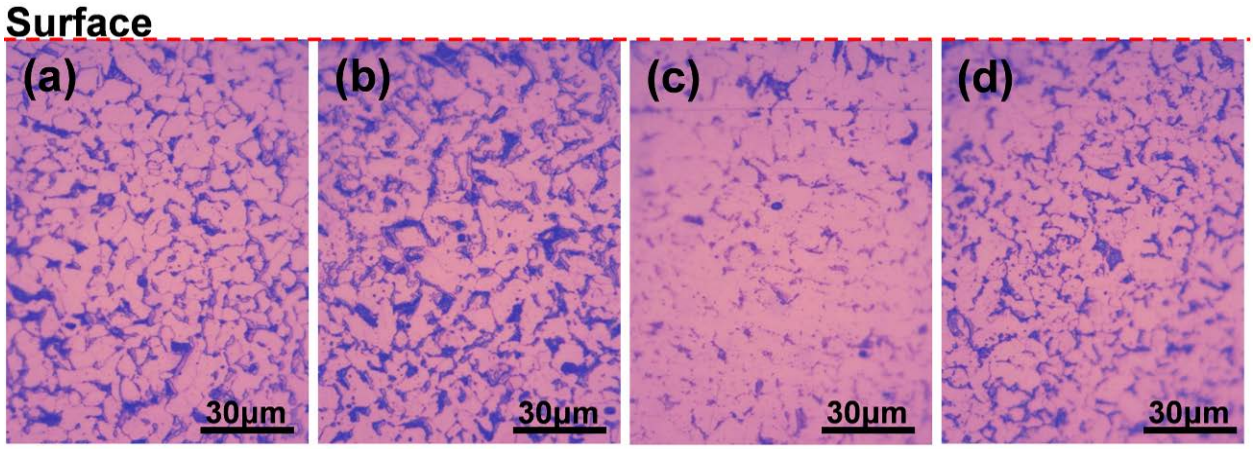

Fig. 10. Optical images of cross-sectional microstructures of CS (a) before and (b-d) after laser peening for (b) one, (c) four, (d) eight impacts.

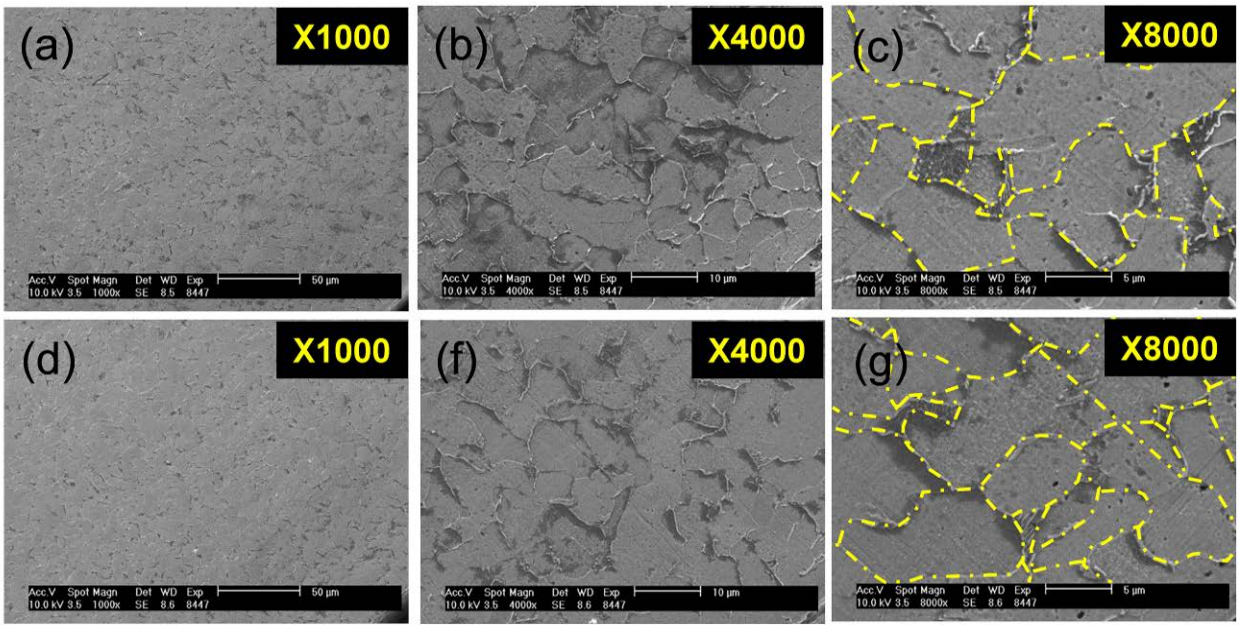

Fig. 11. Different magnified SEM images of cross-sectional microstructures of CS (a-c) before and (d-g) after laser peening for eight impacts.

B. TEM observation

After laser peening, different sorts of defects generated inside the grains of the metal/alloy samples, which have a direct relationship to residual stress and SCC resistance. TEM is the most effective method for observing the small structures/defects inside the grains, such as dislocations, stacking faults, and twins. Since TEM sample preparation and observation are quite complicated and time-consuming (see Section 4.1.3 for detailed TEM sample preparation procedures), we started the research by comparing the 304SS samples with and without large-area LSP for 8 impacts. Only the laser-peened surface was observed, which was expected to show the most obvious microstructure changes according to the microhardness measurement results.

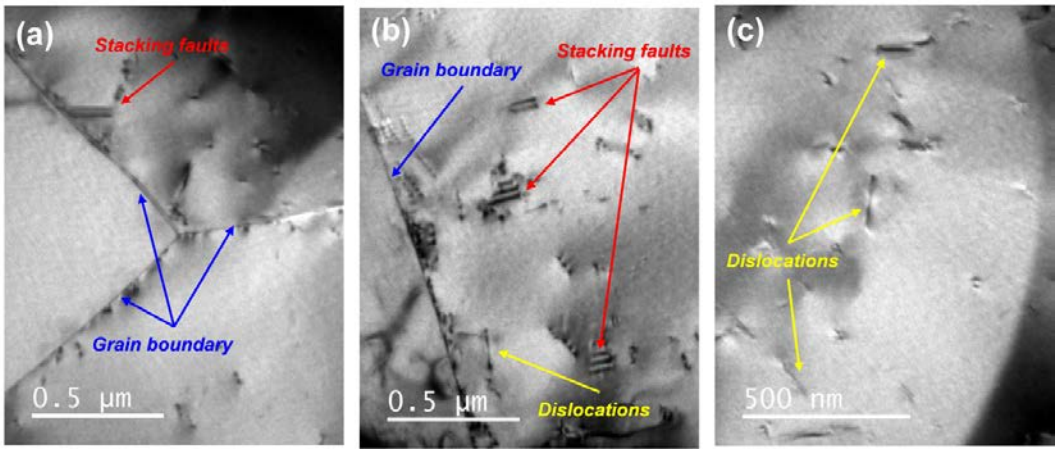

Fig. 12. Typical TEM images of 304SS without laser peening.

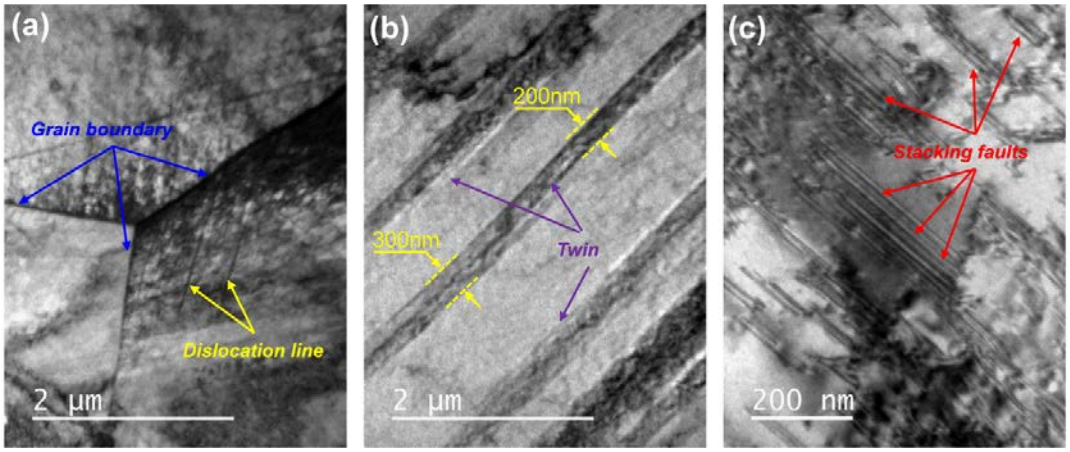

Fig. 13. Typical TEM images of 304SS subjected to eight LSP impacts.

Figure 12 shows some typical TEM images of the grains in the surface layer of the as-received 304SS sample, in which few microstructure features can be identified. In Fig. 12(a), an intersection of three grain boundaries is shown, in which most of the areas are free of defects and some point defects exist near the grain boundaries. In Fig. 12(b) and (c), some stacking faults and dislocations appear. In comparison, TEM images of the surface of the 304SS sample after eight LSP impacts are displayed in Fig. 13. Fig. 13(a) shows the intersection of three grain boundaries, where many black lines appear, and they are especially intensive around the boundaries. These structures should be the increased amount of dislocations. In Fig. 13(b), some lamellar structures with widths of 200 to 300 nanometers were observed, which are suspected to be twins. However, an electron diffraction pattern is needed to confirm it in the future. In Fig. 13(c), plenty of stacking faults were observed. In conclusion, three typical deformation-induced microstructural features were identified in the 304SS sample subjected to eight large-area LSP impacts: dislocations, twins, and stacking faults. The defect generation, such as the dislocation density increase, will result in an increase in hardness and compressive residual stress, which confirms the microhardness results we have measured. The confirmation of defects such as twins and more quantitative results of defect density changes need to be studied further by more experiments in the next reporting period.

4.2.3 SCC constant load testing and analysis

A number of experimental procedures have been developed to assess susceptibility to SCC. Results from these tests can be used to compare the SCC susceptibility of different metals. One of the most widely used SCC assessment methods is the uniaxial constant load test, conducted in accordance with NACE-TM-0177.[4] In this reporting period, the sample preparation and pre-experiment have been done for the SCC constant load test.

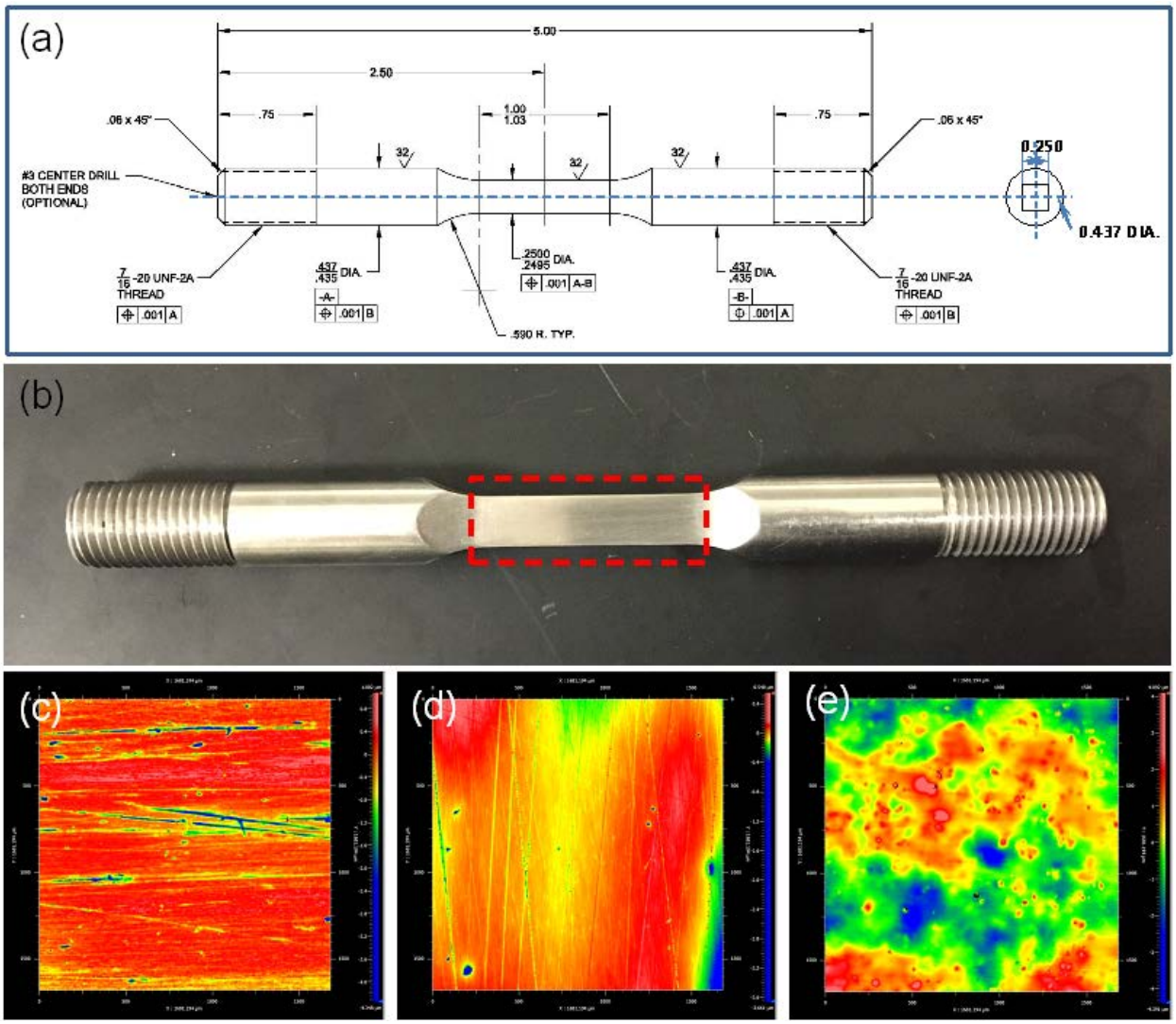

Fig. 14. The (a) drawing and (b) actual 304SS sample for SCC tests. (c) 3D surface topographies of 304SS sample (c) before polishing, (c) after mechanical polishing, and (e) after electrochemical polishing. (Roughness for (c-e) is 266, 69, and 863 nm, respectively.)

First, the sample in the round dog-bone shape was manufactured using 304SS according to the drawing shown in Fig. 14(a). Figure 14(b) displays a photograph of the actual test sample. Second, the testing area marked with dashed red lines was processed in turn by mechanical polishing to remove large scratches and electrochemical polishing to remove small defects and surface residual stress. Typical surface morphologies of test samples before polishing, after mechanical polishing, and after electrochemical polishing are shown in Fig. 14 (c), (d), and (e), respectively. The surface roughness decreased from 266 to 69 nm after mechanical polishing. However, after electrochemical polishing, the surface roughness increased to 863 nm. It should be noted that the sample surface after electrochemical polishing was even more shiny, while there were some newly developed dents resulting in an increase in roughness. Thus, the electrochemical polishing removed small scratches, but it needs to be further optimized (solution

composition, temperature, current, and polishing time) to avoid generating defects itself and to obtain a better surface.

During this reporting period, an initial SCC test was conducted using a 304SS sample without laser peening. The sample was installed in the proof ring and tested with a simulated environment: a test solution consisting of 44.2% $MgCl_2$ dissolved in distilled water at a boiling temperature of 144°C and with applied stress of 300 MPa. After 48 hours, the sample was taken out of the proof ring and characterized using an optical microscope. Two typical corrosions were observed on the test samples: pitting and SCC, as shown in Fig. 15 (b) and (c). A close examination revealed that the SCC initiated at the pitting points and propagated perpendicular to the applied stress, indicating that corrosion pits are the main potential sites for surface crack formation. The stress concentration in the pits will give rise to crack formation and subsequent propagation. Since the SCC was initiated within 48 hours under the selected conditions, we can make use of the current condition for further SCC testing and investigation of the effect of laser peening on SCC.

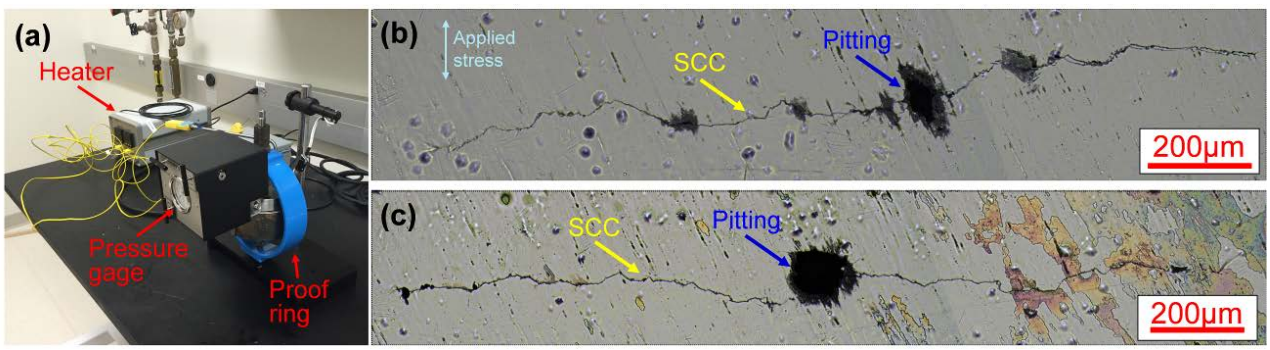

Fig. 15. (a) Experimental setup of proof ring for constant load test s(CLT) . (b) and (c) Two typical optical images of original 304SS sample with SCC test load of 300 MPa and duration of 48 h, which show pitting and SCC cracks.

5. Key outcomes

During this reporting period, the microhardness distribution of laser-peened samples along the near-surface region and the depth direction have been investigated. In addition, the microstructural features of the laser-peened samples have been characterized by OM, SEM, and TEM. Finally, an initial study on the effects of LSP on SCC has been carried out. Some important conclusions have been summarized as follows:

(1) The cross-sectional microhardness distribution of 304SS samples treated by multiple single-spot LSP impacts has been investigated. It was found that the microhardness decreases rapidly with increased depth. The increment of LSP impacts has remarkably improved the microhardness at different depths ranging from 100 to 900

μm. The near-surface and dent center region has the maximum values of microhardness.

(2) The cross-sectional microhardness distribution of 304SS treated by multiple large-area LSP impacts has also been investigated. It was found that the microhardness of 304SS along the surface direction increased rapidly from the no-LSP area to the LSP area. The the greater the number of LSP impacts, the higher the microhardness in the LSP area. For one, four, and eight LSP impacts, the average microhardness is 2.24, 2.47, and 2.70 GPa, respectively, which are approximately 1.1, 1.2, and 1.3 times higher than that of the no-LSP area (2.04 GPa). Along the depth direction, the microhardness of 304 SS decreased rapidly with the increased depth. For carbon steel, the microhardness along the surface and depth direction increased a little with the increment of LSP impacts, much lower than that of 304SS.

(3) A metallographic investigation was performed for 304SS and carbon steel by OM and SEM. The 304SS sample displayed austenite structure, while the CS had two phases of ferrite and pearlite. The average grain size of the 304 SS without laser peening was about 10.5 μm, which decreased to 9.84, 8.9, and 8.82 μm after LSP for one, four, and eight impacts, respectively. Therefore, the decrease in grain size (grain refinement) contributed to the increase in microhardness. The nearly unchanged grain size of the CS agreed well with the tiny change in the microhardness before and after LSP processing.

(4) TEM observation indicated that three typical deformation-induced microstructural features were identified in the 304SS sample subjected to multiple large-area LSP impacts: dislocations, twins, and stacking faults. The defect generation, such as the dislocation density increase, increased the hardness, which confirmed the microhardness results we have measured.

(5) The sample preparation for the SCC test has been carried out. In addition, an initial SCC test was conducted using a 304SS sample without laser peening. After 48 hours of the SCC test at a boiling temperature of 144 ^{o}C and with the applied stress of 300 MPa, two typical corrosions were observed: pitting and SCC. It was also found that the SCC initiates at the pitting points and propagates perpendicular to the applied stress, which indicates that corrosion pits are the main potential sites for surface crack formation.

(b) Description of any Problems/Challenges

No problems were experienced during this reporting period.

(c) Planned Activities for the Next Quarter

The specifically planned objectives and activities to be accomplished during the next period (July 1, 2015, to September 30, 2015) are as follows.

Table 4. The planned objectives and activities for the second quarter.

Objectives	Activities
(a) The corrosion resistance test of laser-peened samples	1) Optimization of LSP processing parameters of samples for the corrosion test. 2) Optimization of corrosion solution and testing conditions. 3) Comparison of the laser-peened and no-laser-peened samples.
(b) Surface evaluation of laser-peened samples	1) To further investigate the grain refinement mechanism of LSP impacts on stainless steel by means of cross-sectional optical microscopy and transmission electron microscopy observation. 2) Quantitative microstructure analysis using electron backscatter diffraction (EBSD) technique.
(c) LSP mechanism study	1) Laser-induced breakdown spectroscopy (LIBS) technique will be used to study LSP process by measuring plasma development and expansion. 2) LIBS will also be used to measure the temperature and density of the LSP-induced plasma. 3) Analysis of LIBS results to demonstrate the LSP processing mechanism.

References

[1] Fairand, B. P.; Clauer, A. H., Effect of water and paint coatings on the magnitude of laser-generated shocks. *Optics Communications* **1976,** *18* (4), 588-591.

[2] Fairand, B. P.; Wilcox, B. A.; Gallagher, W. J.; Williams, D. N., Laser shock - induced microstructural and mechanical property changes in 7075 aluminum. *Journal of Applied Physics* **1972,** *43* (9), 3893-3895.

[3] Caslaru, R.; Guo, Y.; Sealy, M.; Chen, S., Fabrication and characterization of micro dent array produced by laser shock peening on aluminum surfaces. *Trans. NAMRI/SME* **2009,** *37*, 159-166.

[4] Marchebois, H.; Dulcy, N.; Cernocky, E. P.; Desadier, C.; Urband, B.; Legay, F. In *NACE TM0177 Method A Uniaxial Tensile Testing: Learnings from Investigations on Test Procedure*, CORROSION 2009, NACE International: 2009.